1985-05

A cool anomaly off northern California - An investigation using IR imagery and in situ data

Rienecker, M.M.; Mooers, C.N.K.; Hagan, D.E.; Robinson, A.R.

Journal of Geophysical Research; p. 4807-481; (ISSN 0148-0227); 90
http://hdl.handle.net/10945/60090

JOURNAL OF GEOPHYSICAL RESEARCH, VOL. 90, NO. C3, PAGES 4807–4818, MAY 20, 1985

A Cool Anomaly off Northern California: An Investigation Using IR Imagery and In Situ Data

MICHELE M. RIENECKER AND CHRISTOPHER N. K. MOOERS

Department of Oceanography, Naval Postgraduate School, Monterey, California

DENISE E. HAGAN

Jet Propulsion Laboratory, California Institute of Technology, Pasadena

ALLAN R. ROBINSON

Center for Earth and Planetary Physics, Harvard University, Cambridge, Massachusetts

Satellite IR imagery and in situ hydrographic data are used to understand better the mesoscale variability of the California Current system and to explore the relation of its surface and subsurface thermal structures. In August 1982, one of the cool filaments commonly seen in satellite IR images during summer off Northern California was sampled hydrographically during an OPTOMA (Ocean Prediction Through Observation, Modeling, and Analysis) cruise. Based on the cool anomaly seen in a series of IR images and the in situ hydrographic data, and based on geostrophic calculations, a jet entrained upwelled coastal water and advected it rapidly through the warmer waters offshore, providing an important cross-shore transfer process. The anomaly was about 50 km wide and extended vertically to about 40 m. The temperature patterns at the surface were well correlated with those to about 30 m; below 50 m, the surface temperature was better correlated with horizontal temperature gradients, i.e., the "thermal wind", consistent with strong horizontal advection by the geostrophic jet. The cool anomaly was also relatively dense. Based on investigation of the T-S properties, the coastal water had been diluted through mixing with Columbia River plume water on the northern edge of the anomaly. Near the temperature front, in the shoreward sampled portion of the anomaly, and just south of the anomaly, interleaving occurred. There was also a surface saline anomaly embedded in the cool anomaly near the temperature front. The location of the temperature front in the in situ data and in the IR imagery corresponded well. The temperature front was tracked in a series of IR images over 2 weeks. The reorientation of the seaward extremity of the anomaly, from westward to northwestward, and the southwestward displacement of its southern boundary at speeds of 2 to 5 km/d were consistent with the propagation of mesoscale features evident in successive quasi-synoptic surface dynamic topography maps. The southwestward displacement was probably also related to surface Ekman transport.

1. INTRODUCTION

The OPTOMA (Ocean Prediction Through Observation, Modeling and Analysis) program is developing an ocean descriptive-predictive system for four-dimensional data assimilation. It is presently focused on the mesoscale variability in the California Current system (CCS). For the ocean descriptive-predictive system development, quasi-synoptic hydrographic surveys are being conducted to understand the kinematics of the mesoscale variability, to develop statistical models, and to test dynamical models. The objectives of this paper are (1) to assess the relationship of surface temperature structure to subsurface temperature structure and flow fields and (2) to relate surface temperature anomalies to the mesoscale horizontal advective and subsurface mass fields. Pursuit of the first objective aids in evaluating the potential utility of satellite IR imagery for the ocean descriptive-predictive system in the CCS. Pursuit of the second objective helps in understanding better the kinematics of the mesoscale flow field of the CCS and the role of horizontal advection in determining its upper ocean mass field.

The instantaneous CCS differs markedly from the classical conceptual picture of a broad, slow climatological mean current. Based on quasi-synoptic maps acquired by the OPTOMA program, the CCS is known to comprise mesoscale eddies, meandering jets, and turbulent filaments [*Mooers and Robinson*, 1984]. Typical flows determined from CalCOFI (California Cooperative Oceanic Fisheries Investigations) cruises include meanders on scales of 100–300 km [*Wyllie*, 1966]. During winter, warm patches or warm-core (anticyclonic) eddies are a manifestation of these meanders [*Simpson et al.*, 1984; *Koblinsky et al.*, 1984; *Huyer et al.*, 1984*b*]. During summer, long filaments of cool coastal water extend offshore, often with associated eddies, as seen in IR images between April and September [*Bernstein et al.*, 1977; *Breaker and Gilliland*, 1981; *Ikeda and Emery*, 1984]. These filaments, which have their origins in the cool, upwelled coastal water, sometimes extend for several hundred kilometers and may have sharp thermal and chemical fronts associated with them [*Traganza et al.*, 1980]. These fronts are important for primary production because nutrient concentrations in the filaments are high adjacent to the sharp gradients. Away from the coast the filaments are often narrow and would not be resolved by the CalCOFI grid. Depending on atmospheric conditions, satellite IR imagery can provide extensive information, in time and space, on the horizontal gradient of surface temperature, a valuable index for tracking feature evolution.

A series of AVHRR (Advanced Very High Resolution Radiometer) IR images from the NOAA 7 polar-orbiting satellite was acquired during two quasi-synoptic hydrographic surveys

Paper number 4C1422.
0148-0227/85/004C-1422$05.00

conducted by the OPTOMA program off Northern California in August 1982. The first survey sampled the offshore portion of a cool filament embedded in an intense jet which flowed with geostrophically estimated speeds of up to 50 cm/s relative to the flow at 450 m [*Mooers and Robinson*, 1984]. Here, this cool feature is examined more closely, using both the in situ data and IR imagery.

2. THE DATA

The cruise OPTOMA 2 produced two separate maps over a 2-week period in August 1982. From July 31 to August 5 the first cruise leg sampled along parallel tracks (Figure 1*a*) separated by about 45 km; along-track station spacing was approximately 9 km. In a similar manner the second cruise leg, from August 9 to 14, sampled the same domain but truncated alongshore and extended onshore (see Figure 12). There were several components to the cruise data. At stations, hydrographic data were obtained from XBT (expendable bathythermograph) or CTD (conductivity, temperature, and depth) casts. Surface water samples provided temperature and salinity data for calibration purposes. In addition, continuous (except during casts) measurements of temperature and conductivity (converted to salinity) were acquired by sensors located 2 m below the sea surface. The Sippican T-4 XBT's used have an accuracy of ± 0.2°C in temperature and 2% (or 5 m, whichever is greater) in depth. The Neil Brown Instrument IIIb CTD sensors have accuracies of ± 0.005 mmho for conductivity, ± 0.005°C for temperature, and ± 1.6 dbar for pressure. Station positions were determined by Loran C fixes and have quoted accuracies to about 0.1 km. A description of the data preparation and processing can be found in *Rienecker et al.* [1984].

Over the rectangular portion of the domain, which was roughly 130 km by 190 km, 85 XBT casts (to 450 m) and 25 CTD casts (4–1500 m, 21–500 m) were acquired. To calculate dynamic height fields, from which geostrophic velocities were obtained, salinity profiles for the XBT temperature profiles were estimated from a mean S(T) relation calculated from the CTD data. *Emery* [1975] discusses the various errors contributing to the uncertainty in dynamic height values. To justify the use of a mean S(T) relation in estimating the dynamic height from XBT temperature profiles, the uncertainty associated with such a calculation should be no larger than that in the dynamic height calculation from CTD's, estimated by Emery to be about 4 dyn cm. By comparing the dynamic height values calculated from the 25 CTD's in the first cruise leg with the dynamic height values inferred from the temperature profiles of the same CTD's and using the mean S(T) relation, it is estimated that the root mean square (rms) error is 4 dyn cm. The uncertainty is small because much of the surface dynamic height structure comes from the differential vertical displacement of the thermocline, which is located between about 100 and 300 m and where the S(T) relation is quite tight, i.e., the requisite, given by Emery, that the standard deviation in salinity is of the order of 0.1 ppt below 100 m is met.

These uncertainties in dynamic height lead to uncertainties in the geostrophic velocity field, as do navigational errors. Typically, the combined error is probably about 5 cm/s or, equivalently, about 10% in the geostrophic jet. The largest uncertainty, though, is undoubtedly associated with the choice of reference level. With T-4 XBT's and 500-m CTD casts, there is no choice, other than 450 m, for a reference level. *Simpson et al.* [1984] found, for a survey in January 1981, about 500 km to the south of the OPTOMA 2 domain, that a reference level of 1000–1500 m was appropriate. From a site in the northwest of the OPTOMA 2 domain, deep current measurements at about 3000 m and below indicate annual average speeds, including the barotropic component of the flow, of the order of 5 cm/s [*Pillsbury et al.*, 1983]. *Broenkow* [1982] compared geostrophically estimated currents with direct measurements about 200 km offshore of central California in August 1980. He found that a 500-m reference level was inappropriate for scales of motion of 100 km and 1 month or less. His results suggested that the zonal level of no motion was near 1000 m and that for meridional flow was near 2000 m. In June 1983, OPTOMA acquired some CTD casts to 3000 m off northern California. Those casts were too widely separated (by 80 km or more) to provide an accurate picture of the effect of the reference level on the synoptic/mesoscale flow field pattern. There was very little shear between 1000 and 1500 m (as also found by *Simpson et al.* [1984]), but at the surface the velocity relative to 1500 m could be up to twice the velocity relative to 450 m. Hence the geostrophic jet speeds quoted for OPTOMA 2 are very likely lower bounds on the true flow, but the horizontal structure of the surface flow field, which was consistent with the SST patterns in IR images, is unlikely to be much changed by a different reference level.

During the OPTOMA 2 cruise, AVHRR images were acquired daily, near 2300 GMT, and processed at the Scripps Satellite Oceanography Facility (SSOF). A concise description of the SSOF routines and procedure for earth location and calibration of the data is given by *Bernstein* [1982]. Cloudy conditions usually prevailed during the OPTOMA 2 cruise. As part of the analysis of the AVHRR data, clouds were identified by visual inspection of the channel 4 (11-μm) image and by using a channel 2 (visible) threshold cloud mask technique, following Bernstein. Cloud-free data for August 3, 4, and 9 were retrieved at the same locations (to within 2 km) at which in situ data were available.

Initially, a multiwavelength atmospheric correction was applied to the AVHRR data from August 9. These corrected temperatures were compared with 21 colocated in situ SST measurements. The regression relation developed by *McClain et al.* [1983] produced a mean difference (in situ minus satellite values) of 0.1°C with a 0.7°C rms scatter, the latter a significant fraction of the temperature variation (about 2°C) over the cruise domain but consistent with the scatter found by *Strong and McClain* [1984]. Other algorithms were tried, but the rms scatter was not reduced significantly. These regression relations produce a correction to the channel 4 brightness temperature based on the difference between the channel 4 and channel 5 (12-μm) temperatures. A single-channel regression was attempted after it was noted that the rms difference between these two channels was only 0.14°C, which is very near the instrument measurement uncertainty for no intervening atmosphere. The regression relation, derived from the in situ SST and channel 4 brightness temperatures for August 9, produced an rms scatter of 0.6°C, which was no better than that obtained by simply subtracting the channel 4 brightness temperatures from the in situ values. In the latter case there was a bias of 2.2°C for 31 data values from August 3 and 4 and a bias of 1.9°C for data from August 9, with an rms scatter of 0.5°C in both cases. With a systematic measurement bias of 2°C identified, it was decided to make no multiwavelength atmospheric correction but simply to shift the AVHRR data by +2°C to agree more closely in value with the in situ data, similar to the procedure used by

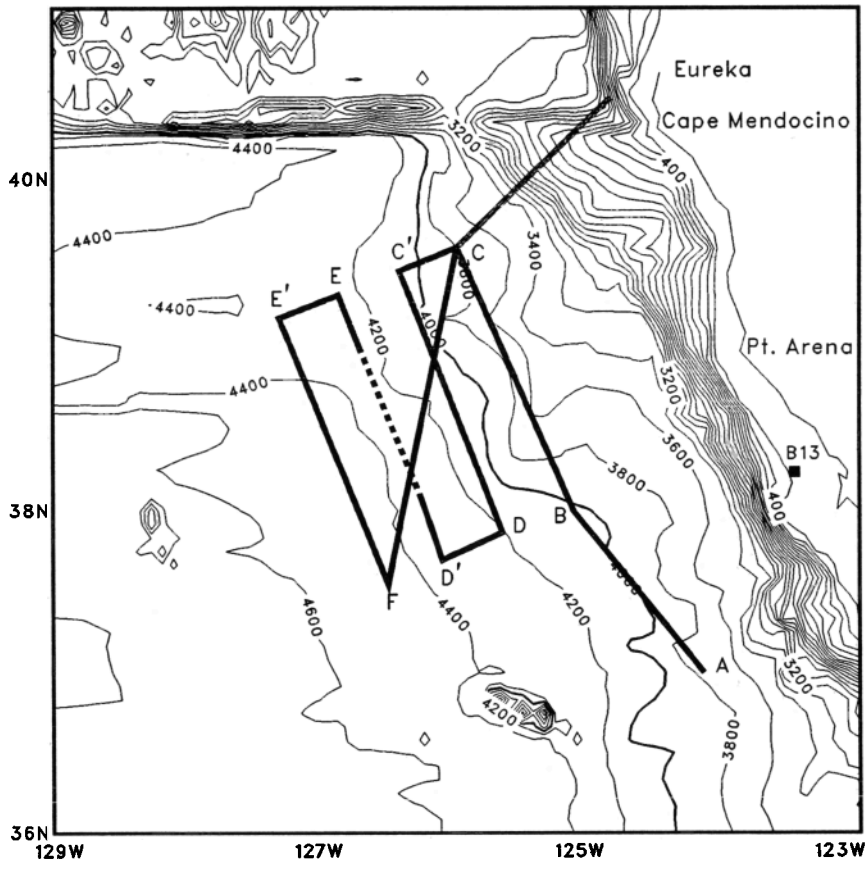

Fig. 1*a*

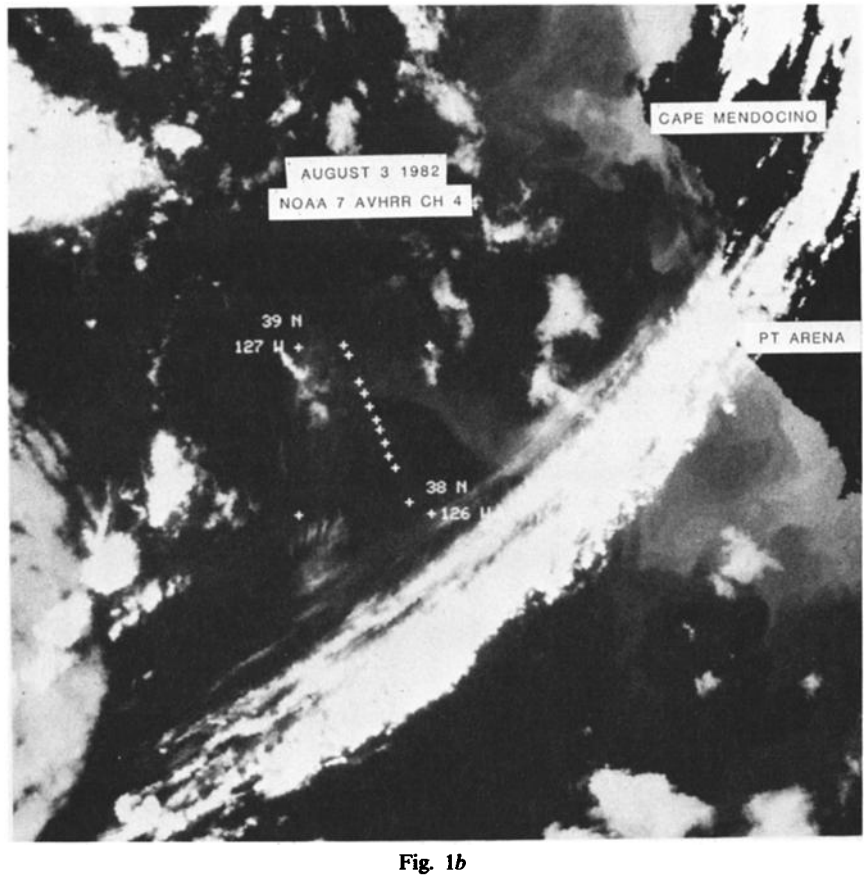

Fig. 1*b*

Fig. 1. (*a*) The OPTOMA 2 cruise track from July 31 to August 5, 1982. The portion of the cruise track displayed on Figure 1*b* is indicated by a dashed line. The location of NDBC buoy 46013 (B13) is identified. (*b*) AVHRR image for August 3, 1982. Part of the transect D'E is shown for reference.

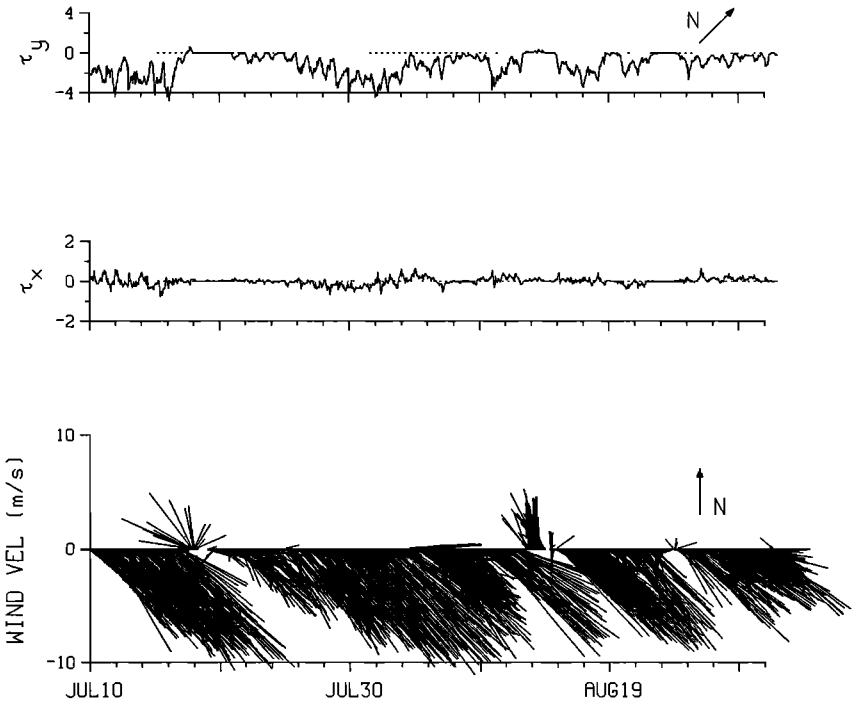

Fig. 2. Hourly wind observations and wind stress components (in dyn/cm^2) at 10 m from NDBC buoy 46013 (38°14'N, 123°18'W) from July 10 to August 31, 1982. The wind vectors are in a N-S, E-W coordinate frame. The wind stress components are in a coordinate frame with the y axis aligned with the direction of the average stress (SE). Negative stress corresponds to downcoast, i.e. equatorward, winds.

Vastano and Bernstein [1984]. This adjustment facilitated visual comparisons of the temperature transects of IR data and in situ data; the AVHRR data were used to examine the horizontal extent and displacement of the cool anomaly encountered during the survey rather than to provide actual SST estimates.

Part of the cruise transect D'E (Figure 1*a*) is superposed on an image from August 3 (Figure 1*b*). The darker shades of grey in the image correspond to higher values of brightness temperature. The satellite sensor has a ground resolution of about 1.1 km at nadir and a noise level of about 0.1°C for the data in the 11-μm channel.

3. THE COOL ANOMALY

During the month of July, prior to the cruise, the winds along the California coast were favorable for upwelling, blowing equatorward, almost parallel to the coast (Figure 2). The upwelled water can be seen in the IR image of August 3 (Figure 1*b*). Clearly linked to the coastal waters is the dominant feature in this image, the cool filament extending far offshore with a sharp temperature gradient (front) at its southern edge.

3.1. *Temperature Structure Along Transects*

The continuous data from the intake sensor at 2 m, the SST from the XBT's and CTD's and the satellite-derived temperatures at the station locations, at roughly 10-km intervals, are compared with temperature transects (Figure 3*a*, *b*, and *c*). Some satellite estimates are absent because of cloud cover. The generally good agreement between the spatial variations of the in situ data and the satellite SST's is encouraging for the integration of these independent data sets in mesoscale studies of the CCS if adequate in situ data are available. The positions for satellite temperatures were colocated to within 2 km of the hydrographic stations; those values for which the difference between the time of the satellite pass and the time of station occupation was more than 3 hours are identified by open circles. For these values, because of the effects of diurnal heating and, possibly, horizontal advection, the lack of synopticity could contribute to the differences between gradients provided by the satellite and hydrographic data. In general the gradients from the satellite data underestimated those from the in situ data, consistent with results of *Maul et al.* [1978], which were attributed to atmospheric moisture effects. Due to lack of resolution, the hydrographic data underestimated the maximum gradient of 2°C/5 km observed in the continuous data along the transect DC' (Figure 3*b*). Along the transect BC (Figure 3*a*), fine structure was encountered as the front was crossed; the maximum gradient within this fine structure was 1.5°C/0.7 km, which was underestimated by both the hydrographic data and the higher-resolution AVHRR data. This gradient is less than that (about 1°C/0.1 km) reported by *Flament et al.* [1983*a*, *b*] from tow-yo CTD measurements across the front on July 24, 1982, during CODE (Coastal Ocean Dynamics Experiment) 2, leg 9.

The near-surface width of the anomaly, based on the location of the 15°C isotherm, varied from about 80 km in the southeast (Figure 3*a*) to about 30 km farther west (Figure 3*c*) and vanished near the western edge of the domain (Figure 4*a*). It decreased with depth, being about 50 km at 50 m in the southeast (Figure 3*a*); overall, the cool anomaly extended to about 40 m; it distorted with depth and was not readily identifiable at 50 m over most of the domain (Figure 4*b*). The upward thermocline displacement under the cool anomaly in Figure 3*c* was due to a cyclone (see Figures 4*b* and 12).

3.2. *T-S Variations and Inferred Water Masses*

Long cool filaments, such as the one evident in the SST field (Figure 4*a*) and the IR image (Figure 1*b*), have frequently been

referred to as plumes. However, from the density field derived from the 2-m data the cool anomaly was also an anomaly of denser water: although there were salinity variations across the cool anomaly, the change in density was dominated by the change in temperature (Figure 3). The combined effect was a sharp density increase across the temperature front; hence the cool feature was not a buoyant plume and, instead, could be referred to as an antiplume.

Within the larger-scale salinity decrease from south to north, across the cool anomaly evident in the top panels of Figure 3, there was a saline anomaly associated with the temperature front. For example, along the transects BC and DC′ where the temperature front was most pronounced, there was a slight increase in salinity on the southern edge of the front followed by a slight decrease on the northern edge (Figure 3*a*, *b*). The region of higher salinity was broader along BC because the first part of this transect ran nearly tangent to the front. (This can be seen in *Mooers and Robinson* [1984, Figure 1].) However, along D′E (Figure 3*c*) the salinity increase spanned a much larger horizontal distance, and the decrease occurred in the northern portion of the anomaly. A negative offshore salinity gradient in the saline anomaly (from BC to DC′) and a positive offshore temperature gradient in the cool anomaly were evident in the continuous data. The broader region of salinity increase along D′E was of higher salinity than along DC′ and was probably due to local upwelling associated with the cyclone center. The 2-m salinity to the south of the saline anomaly had the same value along DC′, D′E, and FE′ (the last not shown). To the north of the saline anomaly, the salinity along BC was the same as that along the other transects, except at the northern extreme, where fresher water was encountered. The maximum salinity values and the sense of the offshore gradients were consistent with the upwelled values measured west of Pt. Arena from July 24 to 26, 1982, during CODE 2, leg 9 [*Huyer et al.*, 1984*a*].

Although they provided only sparse coverage of the study domain, the CTD data were used to determine if different water masses influenced the horizontal structure in the 2-m salinity. The T-S relation in the OPTOMA 2 data was most variable in the upper 75 m of the water column, as can be seen from the T-S curves (plotted with data at 5-m intervals) from six individual CTD casts (Figure 5). These casts give a fair representation of the T-S variation across the domain (Figure 6). There were two casts of type I and 11 of type II; the latter were slightly more saline than type I in the upper 75 m. Three casts of type III to the south of the cool anomaly had fresher water beneath more saline surface water. The four casts of type IV had more complicated structure; they are grouped together because of similarities in the variations of the T-S relation rather than because the T-S relation for each was the same with depth. Two casts to the east had high-salinity surface water above fresher water at 30 to 40 m. To the north and south of the cool anomaly, two casts displayed complicated interleaving of saline and fresh water 30 to 75 m below fresher surface water. Two casts of type V at the western extent of the anomaly displayed warm saline intrusions from about 20 to 75 m. Two casts of type VI near the center and to the southwest of the cyclone showed no interleaving; neither did the cast just to the south that was in transition between the more saline water associated with the cyclone and the fresher water to the south. The existence of complicated interleaving structures and warm, saline intrusions associated with the cool anomaly, its temperature front, and the cyclone was also reported by *Flament et al.* [1983*a*, *b*].

From the results summarized in Figures 5 and 6, the offshore portion of the cool anomaly sampled by OPTOMA 2 was probably influenced by the Columbia River plume. This plume of warm, fresher water may sometimes extend as far south as San Francisco, and the inshore boundary of the plume may be indistinguishable from the seaward boundary of the cool upwelled water [*Huyer*, 1983]. The influence of the Columbia River water mass was evident in the T-S relation for the upper 50 m in the northern portion of a similar cool anomaly sampled closer inshore in early July 1981 [*Olivera*, 1982]. From the OPTOMA 2 data the fresher water in the south of the domain (Figure 6) indicates that the Columbia River water mass influenced the ambient field. The effect of the more saline coastal water was still evident along the temperature front of the cool anomaly. To the south and in the west of the anomaly's offshore extremity, the higher salinity was probably due to the cyclone as well as to the positive background surface salinity gradient offshore and southward caused by the lessened influence of the Columbia River plume water. On both sides of the cool anomaly there was a transition to fresher water; the water just south of, in the east of, and at the western extent of the anomaly displayed interleaving, suggestive of active mixing.

3.3. *Variation of Horizontal Temperature Patterns With Depth*

In the horizontal patterns of the SST field from the in situ data (Figure 4*a*) the cool anomaly, prominent in the IR images, is evident; strong gradients mark the southern edge of the anomaly, and gradients to the north are weaker. The patchiness in the cool anomaly was probably due to differential heating rather than mixing or separate upwelling events because the 2-m salinity at the minimum temperature along BC and DC′ did not vary. The surface temperature front was maintained by the confluence of the surface geostrophic velocity just to the southeast of the center of the domain (Figure 7). Except for the offshore extremity, which was entrained by the cyclone to the west of the domain, the axis of the anomaly lay roughly along the axis of the geostrophic jet directed offshore to the northwest: the cool coastal waters were swept offshore by a jet with speeds of up to 50 cm/s at the surface, relative to the flow at 450 m. The jet had a surface width of about 50 km and extended to 200 m (Figure 8), although at this depth it was considerably weakened, with maximum speeds of 12 cm/s relative to 450 m. The axis of the jet was tilted and narrowed with depth; at 200 m it was displaced about 20 km (Figure 8) to the northeast (based on maps not shown) relative to its surface location.

The relationship of the temperature structure in the IR imagery to the horizontal temperature structure at depth is of interest. In the absence of a quantitative gridded SST field derived from the IR imagery, and because of the close relationship between the structure in the IR imagery and the in situ SST field, the latter was used instead in the correlation calculations described below. Pattern correlations of the in situ SST field with the horizontal temperature fields at different depths (Figure 9) show a sharp decrease in correlation with increasing depth. Based on the 110 sample points of the first cruise leg, the correlation at 30 m was 0.49 and that at 50 m was 0.10, the latter not significant at the 95% level, using an estimated 30 degrees of freedom [*Davis*, 1976].

Two-dimensional, spatially lagged correlations (of spatially binned data, with 10 by 10-km bins) between SST and the temperature at depth revealed no pattern consistent with the

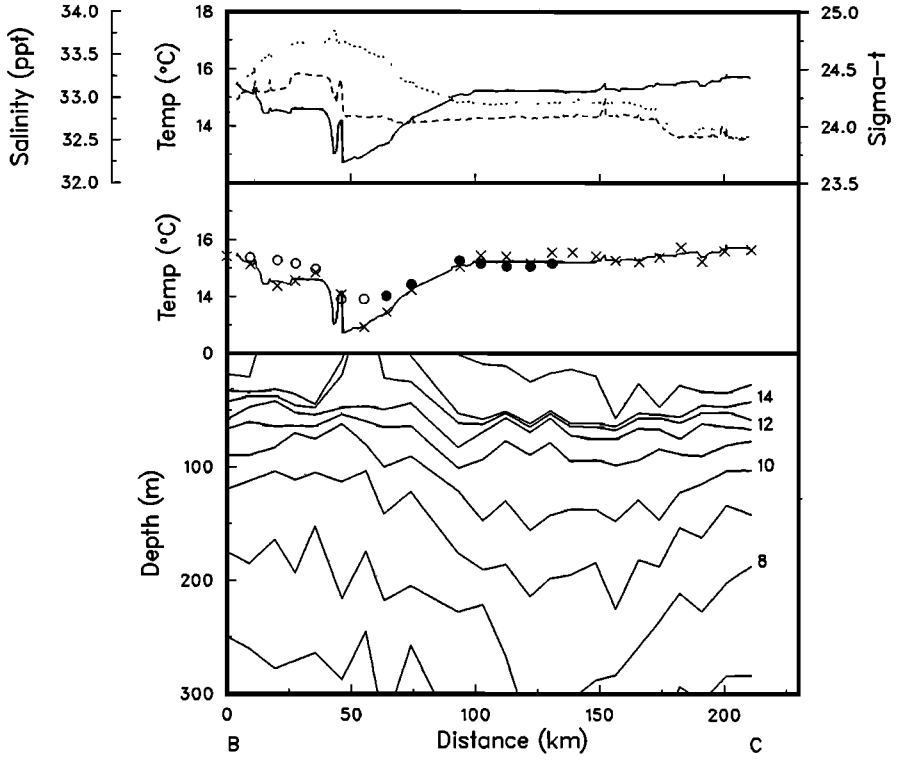

Fig. 3*a*

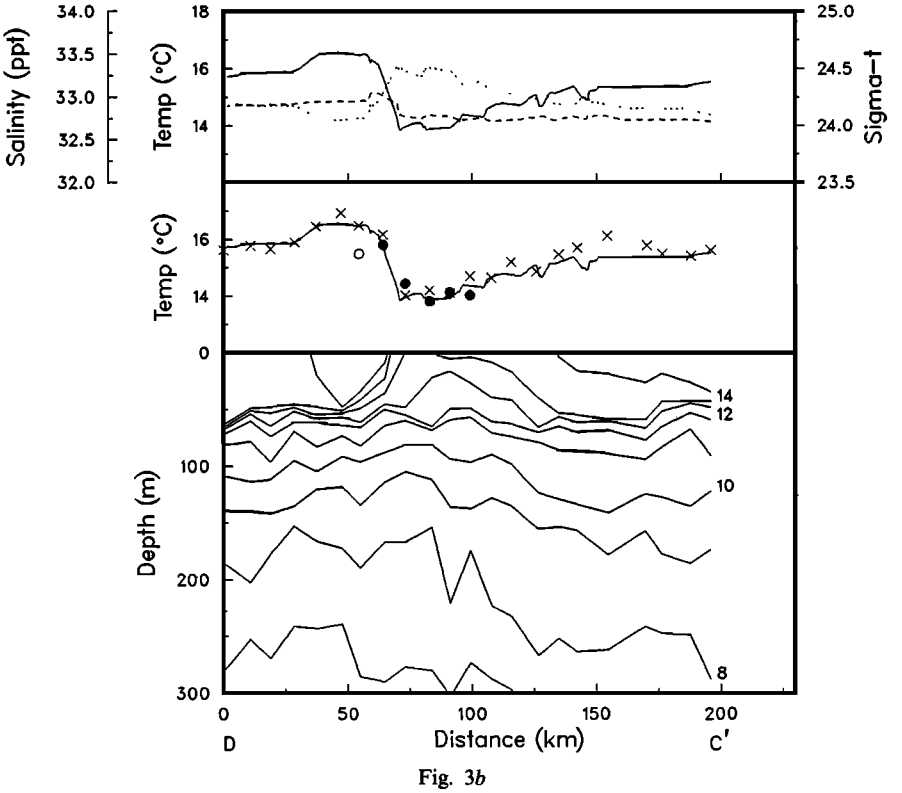

Fig. 3*b*

Fig. 3. Temperature transects (*a*) BC, (*b*) C'D, and (*c*) D'E. The temperature data from the 2-m sensor (solid line), the XBT's and CTD's (×), and the satellite sensor (solid and open circles) are shown above the isotherm plots. The open circles identify positions for which there was a time difference greater than 3 hours between the satellite pass and station occupation. The top panel shows temperature (solid line), salinity (dashed line), and sigma-t (dotted line) from the 2-m sensor.

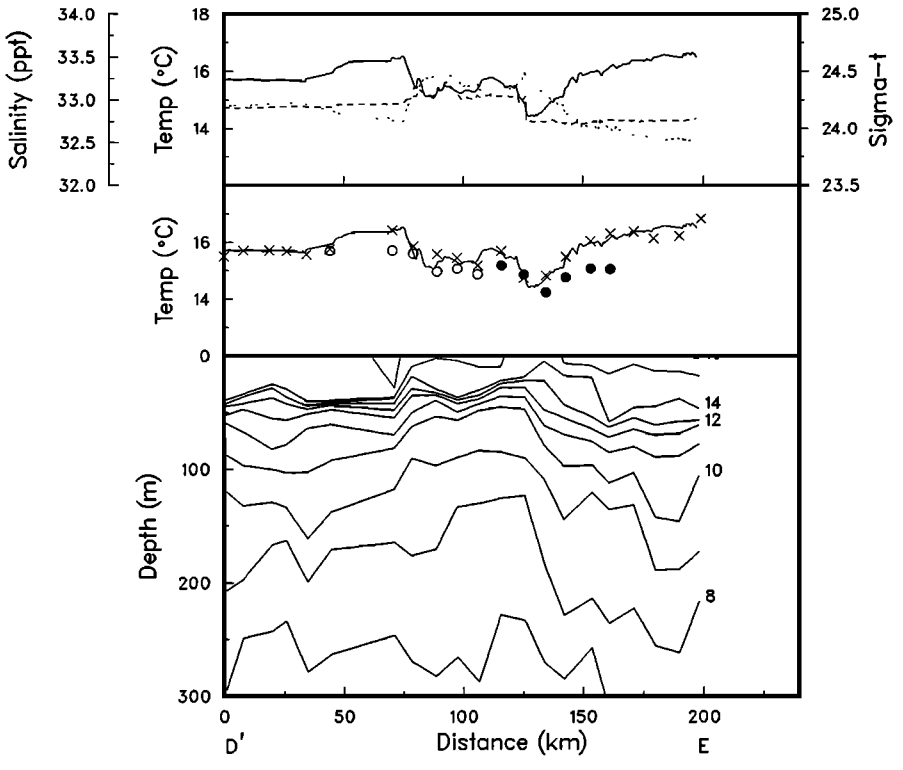

Fig. 3c

geostrophic current axis tilt, and the maximum correlation was only about 0.25 for SST with the temperature at or below 50 m. Cool features in the temperature field at 30 m (not shown) were clearly related to the surface anomaly; but at 50 m (Figure 4*b*) the anomaly was no longer evident over most of the domain, and the structure was entirely changed, reflecting more the vertical displacement of the thermocline. In contrast to the SST field, the temperature pattern at 50 m was well correlated with the pattern below, down to 400 m (Figure 9). The pattern correlation of the surface dynamic topography

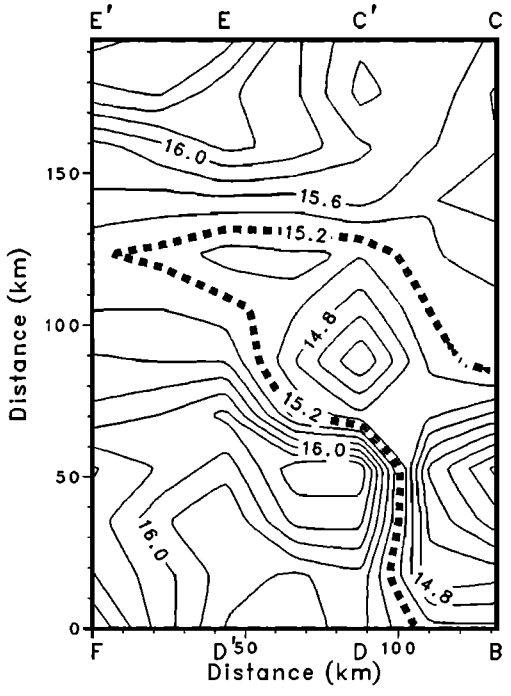

Fig. 4a

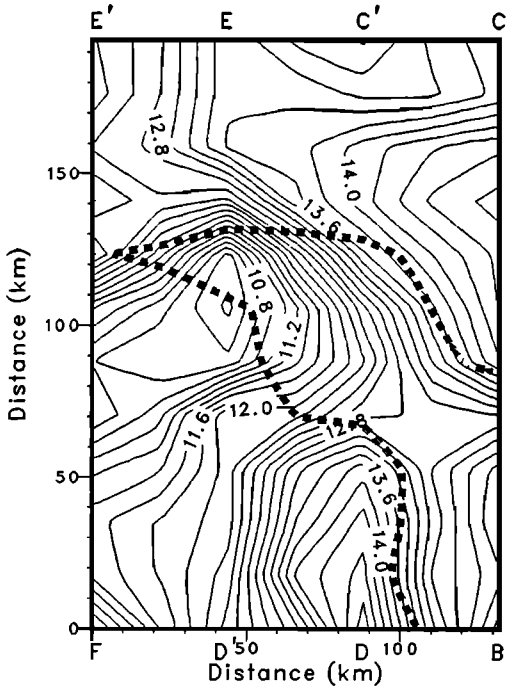

Fig. 4b

Fig. 4. Temperature fields based on the hydrographic station data. The contour interval is 0.2°C. The contour for 15.2°C is highlighted and used to identify the cool anomaly on Figures 6 and 7. The transect extremes are identified by letter. The rectangle is oriented nearly 20° west of north, with origin at 37°33'N, 126°25'W. (*a*) SST; (*b*) temperature at 50 m, with the 15.2°C contour from SST superposed.

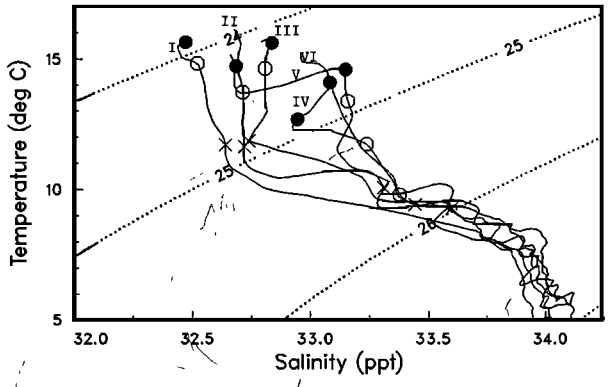

Fig. 5. Representative T-S curves. I shows the influence of the fresher Columbia River plume water, II and III show the transition to the higher-salinity water along the cool anomaly IV, V, and VI (see Figure 6 for locations). The T-S pairs at 30 m (solid circles), 50 m (open circles), and 75 m (cross) are marked.

with the temperature at the surface was 0.0, with the temperature at 100 m, 0.89 and with that at 200 m, 0.86. Reflecting the correlation between dynamic topography and temperature at depth, the SST field was better correlated with the horizontal temperature gradient field at depth: the modulus of the complex correlation between SST and the complex horizontal temperature gradient ($\partial T/\partial x + i\,\partial T/\partial y$, with $i = \sqrt{-1}$) was maximum when the gradient was lagged 20 km to the north of the surface temperature points. The modulus of the correlation increased with depth and was 0.5 at 200 m (Table 1). At this depth the direction of maximum correlation was roughly perpendicular to the jet axis, as is to be expected from the "thermal wind" relation. The modulus of the correlation at zero lag was about 0.3 below 100 m. Thus, although it seems difficult, based on IR images alone, to determine a priori at what depth the variable correlated with SST changes from temperature to the horizontal temperature gradient, the patterns in these IR images are related to temperature structure at depth.

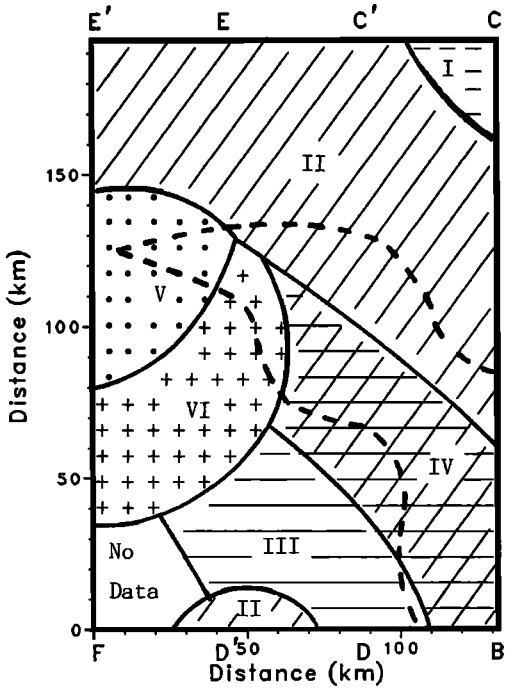

Fig. 6. Water type regions defined by Figure 5. The cool anomaly as defined by the 15.2°C contour is outlined.

From a similar study [*Van Woert*, 1982] in the North Pacific Subtropical Frontal Zone during winter conditions, the surface and subsurface temperature fields were significantly correlated above 800 m, except at the base of the mixed layer and near a depth of 500 m, where there was a shallow salinity minimum. The difference between the two situations is highlighted by the different correlations of surface temperature with surface dynamic topography: in the Fronts 80 data set [*Van Woert*, 1982] the zero-spatial-lag correlation was 0.65; in the present data set the correlation was nil, as noted above. The SST pattern during Fronts 80 reflected the variable depth of the thermocline as a result of a deep wintertime mixed layer, whereas the SST pattern sampled by the OPTOMA 2 cruise was determined by summertime heating, upwelling, and advection by the mesoscale flow field.

3.4. *Synoptic Information From IR Data*

Since cruise data are quasi-synoptic, IR imagery can extend the usefulness of these data by providing a time series of synoptic views of the surface structure. The correspondence between the features in the IR imagery and those in the in situ data provides confidence for relating changes in the series of images to changes observed from the first map (from August 1 to 4) to the second map (from August 9 to 12). A comparison of the images from August 3 and 9 (Figures 1*b* and 10, respectively) shows changes in the orientation and position of the cool anomaly. The locus of the southern edge of the temperature front, determined by the largest change in temperature across two adjacent pixels, was tracked in the series of images (Figure 11); some of the curves are truncated as a result of cloud cover. The offshore extremity of the front rotated to a north northwest orientation, consistent with the rotation of the jet axis (see below) seen in a comparison of dynamic height fields from the first map (the large domain) and the second

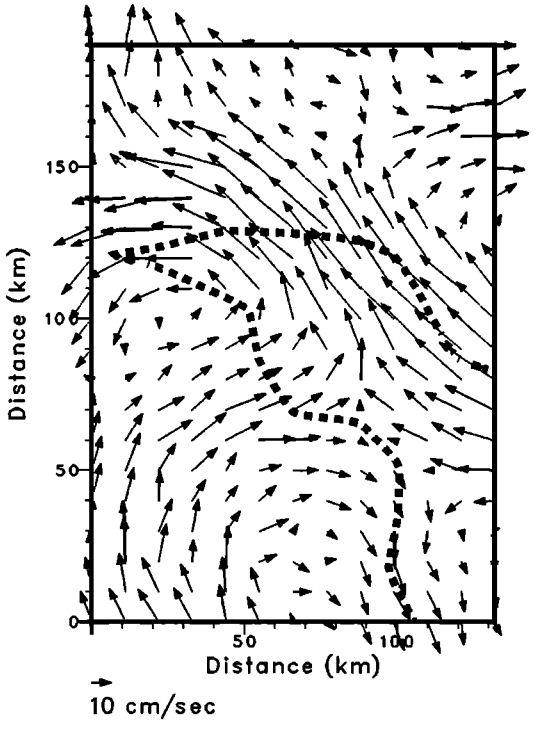

Fig. 7. Surface geostrophic velocities relative to 450 m. The surface cool anomaly, as defined by the 15.2°C contour, is shown. The domain is the same as in Figure 4.

map (Figure 12). The front also moved southwestward, at least partially consistent with southwestward displacement of the southern portion of the jet and anticyclone; the latter was evident in the second map, and its existence during the first map was inferred by a comparison of the fields in Figure 12. *Mooers and Robinson* [1984] estimated the propagation speeds of the mesoscale eddies evident in the dynamic height fields. Between the first and second maps, the main cyclone moved northwestward at a rate of 8–12 km/d; this eddy was located at the offshore extremity and slightly to the south of the anomaly, and its movement was probably the main reason for the reorientation of the cool anomaly. Due to the truncation of the domain in the south and the southwestward displacement of the anomaly, the distinctive surface temperature front was not sampled in the second leg of the cruise.

The apparent eventlike displacement of the front, as seen in Figure 11, is slightly misleading because of the truncated locus for August 5 and missing data for August 6 to 8, when satellite passes were not archived at SSOF. One image, for August 6, was available from the NOAA/NESDIS facility at Redwood City, and in it the cool anomaly and associated front were still prominent. Because the time scale of frontogenesis in the open ocean or for offshore advection of new frontal features is longer than 2 days, and because multiple fronts were not evident in the data (Figure 3), it seems certain that the loci traced in Figure 11 were for the same front. There was definitely a larger southwestward displacement (difficult to determine unambiguously but estimated to be about 30 km on average) between August 4 and 9 than between days prior to August 4 or after August 9. This "event" could have been associated with the generally stronger winds experienced on August 8 and 9 than on the days before or after (see Figure 2). A simple Ekman response model, with the wind stress forcing shown in Figure 2 and assuming an average mixed layer depth of 30 m, predicts a southwestward displacement of 21 km from August 4 to 10; the displacement from August 9 to 10 was 2 to 3 times larger than on the previous days; the prevailing winds caused an average displacement of about 3 km/d from August 4 to 9, whereas the displacement from August 9 to 10 was about 10 km. Since the winds offshore are generally stronger than those

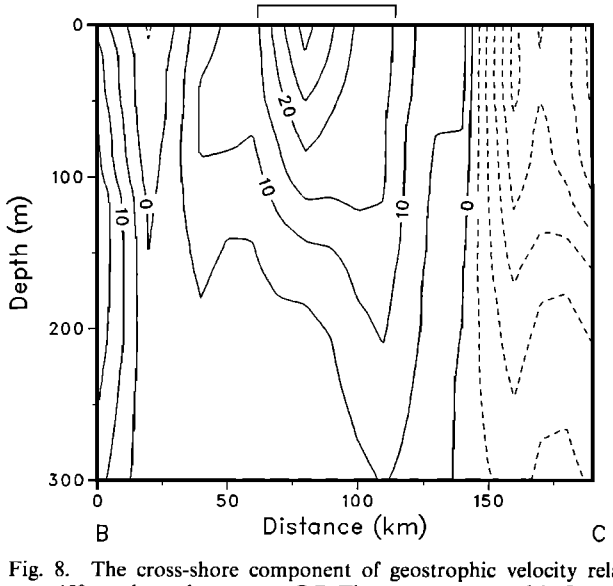

Fig. 8. The cross-shore component of geostrophic velocity relative to 450 m along the transect BC. The contour interval is 5 cm/s. The surface extent of the jet which advects the cool anomaly offshore is indicated.

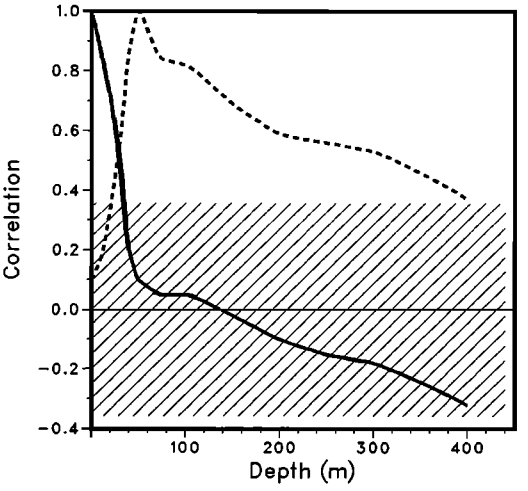

Fig. 9. Pattern correlations from the in situ data. The cross-hatched region depicts the 95% significance level for 30 degrees of freedom: (solid line) correlation of SST with temperature at depth, (dashed line) correlation of temperature at 50 m with temperature at depth.

near the coast, if the wind event at the coastal buoy occurred several hours to a day later than a similar offshore event, then it seems plausible that the larger displacement between August 4 and 9, evident in Figure 11, was due to local atmospheric forcing.

4. Discussion and Conclusions

From the theoretical results of *Ikeda and Emery* [1984] it is probable that current meanders are triggered by topography close to the California coast and grow as a result of the baroclinic instability of the coastal equatorward surface jet (associated with coastal upwelling) and the poleward California Undercurrent (CU). Such unstable meanders sweep the cool water offshore and often lead to isolated eddies or vortex pairs [*Bernstein et al.*, 1977]. However, the dynamical cause of the eddies whose surface signatures are apparent in IR images in summer off California has not been clearly established. Other contending or contributing production mechanisms include instabilities of the offshore CCS itself and processes related to wind stress and its curl and variability and irregularities in

TABLE 1. Correlation of Spatially Binned Data of $T(x, y, 0)$ With $(\partial T/\partial x + i\partial T/\partial y)(x + \Delta x, y + \Delta y, d)$

Depth d	Lag $(\Delta x, \Delta y)$	Correlation Modulus	Correlation Direction
50 m	(0, 0)	0.28	130°
	(10, 20)	0.50	168°
100 m	(0, 0)	0.33	154°
	(10, 20)	0.51	171°
150 m	(0, 0)	0.30	179°
	(0, 20)	0.50	189°
200 m	(0, 0)	0.36	182°
	(0, 20)	0.51	195°
250 m	(0, 0)	0.35	171°
	(0, 20)	0.41	185°
300 m	(0, 0)	0.34	173°
	(0, 20)	0.39	187°
400 m	(0, 0)	0.27	190°
	(0, −20)	0.39	186°

The zero-lag and maximum-modulus-lag correlations are shown. The direction is measured clockwise from north. The data were objectively analyzed fields on a grid with 10-km spacing.

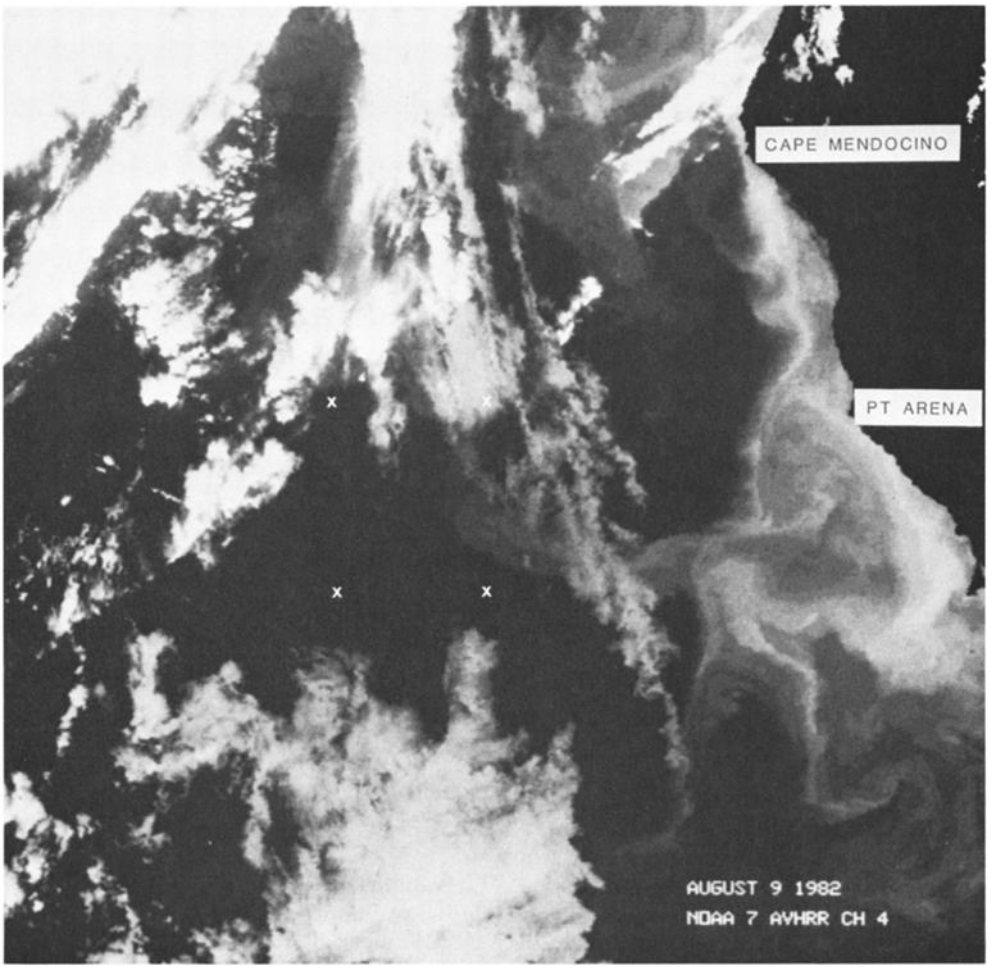

Fig. 10. AVHRR image from August 9, 1982: The crosses (×) show the intersections of 38 and 39°N with 126 and 127°W, as in Figure 1*b*.

bottom topography and coastline features. For example, one eddy-eddy-jet interaction observed by OPTOMA in summer 1983 [*Robinson et al.*, 1984] showed characteristics of barotropic instability. Comparisons of in situ data and information yielded by IR imagery with theoretical models may identify features or indices that could be regularly monitored; the resultant space-time series would be valuable for the understanding of eddy dynamics in the CCS.

The information content in each data set, either in situ or remotely sensed, is very different, but each complements the other. The in situ data provide accurate measurements of the temperature and density structure with depth and an insight into the dynamics. The results of the water mass analysis presented here emphasize the value of having salinity as well as temperature data. Satellite-derived SST's, however, provide repeated synoptic measurements over large areas and help interpret more fully the results of intermittent, limited-area, quasi-synoptic maps made by ships; for example, the IR images presented here served to link the cool anomaly found in the in situ data offshore to the coastal upwelling regime and the offshore geostrophic jet and to describe its displacement during two cruise legs conducted over 2 weeks. Hence, it is in their space-time patterns that the IR images provide the most useful information.

Here the data sets were used in conjunction with each other in a qualitative way: the in situ data aided in the interpretation of the imagery patterns, indicating that the cool anomaly comprised cool, saline coastal water advected offshore by the intense jet and also that the surrounding warm, fresher waters were entrained into the turbulent jet and mixed with the anomaly, possibly with the aid of advection by mesoscale eddies. The imagery provided a means to extrapolate in time and space the understanding of the processes at work in the smaller study domain to a large, regional domain.

The cool anomaly, seen to persist from a well-developed state in IR images in mid-July to a much weakened state (with smaller temperature gradients over narrower regions) in IR images in mid-August 1982, was found by investigation of in situ data to be an anomaly of denser water as well. The anom-

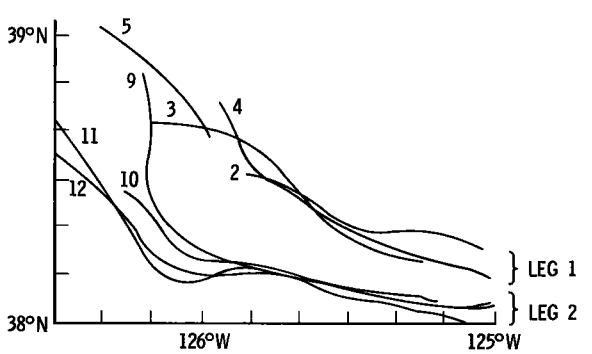

Fig. 11. Loci of the temperature front as determined from the series of IR images. Curves are labeled with dates in August 1982.

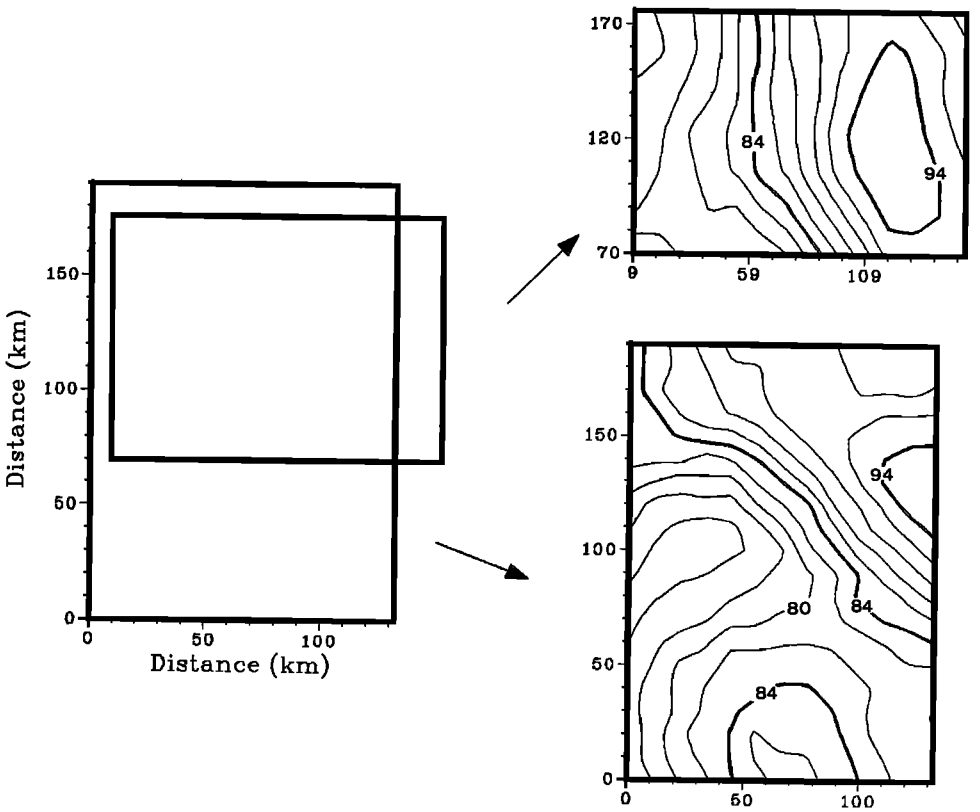

Fig. 12. On the left is the superposition of the two study domains of OPTOMA 2, the larger is the first cruise leg domain of August 1–4; the second cruise leg domain was covered from August 9 to 12. On the right are the corresponding surface dynamic topography maps, relative to 450 m. The contour interval is 2 dyn cm, and the contours for 84 dyn cm and 94 dyn cm are highlighted (following *Mooers and Robinson* [1984]).

aly, which extended to a depth of nearly 40 m and had a width of about 50 km, was advected offshore by an intense jet that extended to a depth of at least 200 m and flowed with speeds of up to 50 cm/s at the surface relative to 450 m. This maximum speed is consistent with independent Lagrangian drifter estimates in the jet [*Flament et al.*, 1983*a*]. The surface temperature front at the southern edge of the anomaly was maintained by confluence in the surface flow field. Displacements of the anomaly, estimated by tracking features in the IR images, were consistent with propagation of mesoscale features and Ekman displacements by local winds. The jet moved westward at about 4 km/d, and the anticyclone seemed to rotate about some northern point so that its southern extent moved southwestward at about 3 km/d; these estimates are in good agreement with the theoretical phase speed of *Ikeda and Emery* [1984]. The main cyclone moved northwestward at about 8 km/d, reorienting the anomaly. In addition, eventlike displacements of the temperature front seemed to be associated with atmospheric forcing events and were consistent with predicted Ekman displacements.

From the depth of penetration of the cool anomaly the temperature pattern to 30 m, but to less than 50 m, could, in this case, have been usefully estimated from satellite-derived SST estimates. The SST was more highly correlated with the horizontal temperature gradient at depth. The weak correlation of the SST with subsurface temperature noted here has occurred in other quasi-synoptic maps made by OPTOMA; however, there have been maps (e.g., OPTOMA 4, a cruise in the same region, from March 24 to April 1, 1983) when the correlation was high. The result depends strongly on the state of the upper ocean, especially on whether or not there is a deep (relative to the main thermocline) mixed layer, which is largely a seasonal property. Thus it is necessary to take into account air-sea interactions to fully exploit the SST information.

Overall, the implications are that modeling, both dynamical and thermodynamical, will be essential to extract the full information content of the satellite-derived SST field for ocean monitoring and prediction. Clearly, the strong relation between the cool SST anomaly and the surface flow field described here makes it worthwhile and essential to undertake such model-satellite IR data integrations in a four-dimensional data assimilation scheme.

Transient wind (atmospheric synoptic-scale) events (Figure 2) strongly influence the coastal upwelling process and, presumably, the quantity and nature of the associated physical and biochemical properties of the cool anomaly's source water. As found in the OPTOMA 2 study, the cool anomaly may be modified through mixing, air-sea transfers, and Ekman displacements. It would be of interest to determine the net onshore-offshore heat and other fluxes, and their divergences, associated with the eddy, jet, and front system; this could be done with an appropriate numerical model, but an adequate data base would be needed for an independent test of the applicability and accuracy of the model. Hence, repeated, finely spaced CTD casts, velocity profiles, and water samples along and across cool anomalies, such as those studied here, as well as near-surface drifter deployments from the coast to a few hundred kilometers offshore are needed.

Acknowledgments. George Halliwell, from Oregon State University, kindly provided the buoy wind data. Jane Huyer, from Oregon State University, provided useful ancillary information and advice.

The careful and thorough reviews by Robert Bernstein and anonymous referees are greatly appreciated. Computer time was provided by the W. R. Church Computer Center at the Naval Postgraduate School. Satellite data processing was accomplished at the Scripps Satellite Oceanography Facility. The R/V *Acania* was essential to the in situ synoptic studies. In part this research was carried out at the Jet Propulsion Laboratory, California Institute of Technology, and was jointly sponsored by the Physical Oceanography Program of the Office of Naval Research and by the National Aeronautics and Space Administration.

REFERENCES

Bernstein, R. L., Sea surface temperature estimation using the NOAA 6 satellite advanced very high resolution radiometer, *J. Geophys. Res.*, *87*, 9455–9465, 1982.

Bernstein, R. L., L. Breaker, and R. Whritner, California Current eddy formation: Ship, air, and satellite results, *Science*, *195*, 353–359, 1977.

Breaker, L., and R. P. Gilliland, A satellite sequence on upwelling along the California coast, in *Coastal Upwelling, Coastal Estuar. Sci.*, vol. 1, edited by F. A. Richards, pp. 87–94, AGU, Washington, D. C., 1981.

Broenkow, W. W., A comparison between geostrophic and current meter observations in a California Current eddy, *Deep Sea Res.*, *29*, 1303–1311, 1982.

Davis, R. E., Predictability of sea surface temperature and sea level pressure anomalies over the North Pacific Ocean, *J. Phys. Oceanogr.*, *6*, 249–266, 1976.

Emery, W. J., Dynamic height from temperature profiles, *J. Phys. Oceanogr.*, *5*, 369–375, 1975.

Flament, P., L. Washburn, and L. Armi, Towyo CTD observations of fronts during CODE using satellite IR images (abstract), *Eos Trans. AGU*, *64*, 718, 1983*a*.

Flament, P., L. Washburn, and L. Armi, Observations of the subsurface structure of an upwelling filament coordinated with a sequence of IR images (abstract), *Eos Trans. AGU*, *64*, 1059, 1983*b*.

Huyer, A., Coastal upwelling in the California Current System, *Progr. Oceanogr.*, *12*, 259–283, 1983.

Huyer, A., J. Fleischbein, and R. Schramm, Hydrographic data from the second Coastal Ocean Dynamics Experiment: R/V *Wecoma*, leg 9, 6–27 July 1982, *CODE, Tech. Rep. 25*, 130 pp., Coll. Oceanogr., Oreg. State Univ., Corvallis, 1984*a*.

Huyer, A., R. L. Smith, and B. M. Hickey, Observations of a warm-core eddy off Oregon, January to March, 1978, *Deep Sea Res.*, *31*, 97–117, 1984*b*.

Ikeda, M., and W. J. Emery, Satellite observations and modeling of meanders in the California Current System off Oregon and Northern California, *J. Phys. Oceanogr.*, *14*, 1434–1450, 1984.

Koblinsky, C. J., J. J. Simpson, and T. D. Dickey, An offshore eddy in the California Current System, 2, Surface manifestation, *Progr. Oceanogr.*, *13*, 51–69, 1984.

Maul, G. A., P. Webb de Witt, A. Yanaway, and S. R. Baig, Geostationary satellite observations of Gulf Stream meanders: Infrared measurements and time series analysis, *J. Geophys. Res.*, *83*, 6123–6135, 1978.

McClain, E. P., W. G. Pichel, C. C. Walton, Z. Ahmad, and J. Sutton, Multichannel improvements to satellite-derived global sea surface temperatures, *Adv. Space Res.*, *2*, 43–47, 1983.

Mooers, C. N. K., and A. R. Robinson, Turbulent jets and eddies in the California Current and inferred cross-shore transports, *Science*, *223*, 51–53, 1984.

Olivera, R. M., A complex distribution of water masses and related circulation off northern California in July 1981, M.S. thesis, 53 pp., Oreg. State Univ., Corvallis, 1982.

Pillsbury, R. D., J. Bottero, G. Pittock, D. C. Root, J. Simpkins III, and G. R. Heath, Data report for current meters on moorings CMMW-5, 6, 7, 8, and 9 1981–82, Pacific study area W-N, *Rep. OSU-20*, 313 pp., School Oceanogr., Oreg. State Univ., Corvallis, 1983.

Rienecker, M. M., C. N. K. Mooers, M. C. Colton, and P. A. Wittmann, Hydrographic data from the OPTOMA program, OPTOMA2, Legs 1 and 2, July 31 to August 14, 1982, *Tech. Rep. NPS68-84-002*, 65 pp., Nav. Postgrad. School, Monterey, Calif., 1984.

Robinson, A. R., J. A. Carton, C. N. K. Mooers, L. J. Walstad, E. F. Carter, M. M. Rienecker, J. A. Smith, and W. G. Leslie, A real-time dynamical forecast of ocean synoptic/mesoscale eddies, *Nature*, *309*, 781–783, 1984.

Simpson, J. J., T. D. Dickey, and C. J. Koblinsky, An offshore eddy in the California Current System, 1, Interior dynamics, *Progr. Oceanogr.*, *13*, 5–49, 1984.

Strong, A. E., and E. P. McClain, Improved ocean surface temperatures from space-comparisons with drifting buoys, *Bull. Am. Meteorol. Soc.*, *65*, 138–142, 1984.

Traganza, E. D., D. A. Nestor, and A. K. McDonald, Satellite observations of a nutrient upwelling off the coast of California, *J. Geophys. Res.*, *85*, 4101–4106, 1980.

Van Woert, M., The subtropical front: Satellite observations during FRONTS 80, *J. Geophys. Res.*, *87*, 9523–9536, 1982.

Vastano, A. C., and R. L. Bernstein, Mesoscale features along the first Oyashio Intrusion, *J. Geophys. Res.*, *89*, 587–596, 1984.

Wyllie, J. G., Geostrophic flow of the California Current at the surface and at 200 m. *Calif. Coop. Oceanic Fish. Invest.*, atlas 4, 13 pp., 288 charts, State Calif. Mar. Res. Comm., San Diego, 1966.

D. E. Hagan, Jet Propulsion Laboratory, California Institute of Technology, Pasadena, CA 91109.

C. N. K. Mooers and M. M. Rienecker, Department of Oceanography, Naval Postgraduate School, Monterey, CA 93943.

A. R. Robinson, Center for Earth and Planetary Physics, Harvard University, Cambridge, MA 02138.

(Received May 29, 1984;
revised October 29, 1984;
accepted November 1, 1984.)